Guided wave energy focusing and steering in composite laminates

F. Hervin, P. Fromme

F. Hervin, P. Fromme, "Guided wave energy focusing and steering in composite laminates," Proc. SPIE 12488, Health Monitoring of Structural and Biological Systems XVII, 1248804 (25 April 2023); doi: 10.1117/12.2657435

SPIE.

Event: SPIE Smart Structures + Nondestructive Evaluation, 2023, Long Beach, California, United States

Guided Wave Energy Focusing and Steering in Composite Laminates

F. Hervin and P. Fromme
Department of Mechanical Engineering, University College London, WC1E 7JE, UK

ABSTRACT

Lightweight, carbon fiber reinforced composites are often selected for aerospace components but are prone to barely visible impact damage, caused by low velocity impacts, during service. Guided-wave-based structural health monitoring (SHM) techniques can efficiently detect impact damage impact in composite structures. However, wave propagation is influenced by material anisotropy resulting in a number of effects. The phase and group velocity of propagating wave modes depend on the wave launching direction, with increased wave speeds in the high stiffness (fiber) directions. Wave energy tends to be focused along the fiber directions, resulting in beam steering or skewing away from the initial wave launching direction. These anisotropic effects, if unaccounted for, could lead to inaccurate localization of damage, and potential regions of the structure where guided waves cannot propagate with sufficient amplitude, reducing damage sensitivity. Wave propagation in an undamaged unidirectional carbon fiber reinforced polymer (CFRP) panel was investigated for the A_0 mode for multiple wave launching directions. Finite Element (FE) modelling was carried out using homogenized anisotropic material properties to investigate the directional dependency of velocity. Point and line sources were modelled to investigate the influence of the excitation source on the guided wave evaluation and signal processing. Wave skewing behavior was visualized for the line source, and wave skew angles and beam spread angles were calculated for a range of propagation angles. Experimental non-contact guided wave measurements were obtained using a laser vibrometer. A PZT strip transducer was developed in order to measure wave skew angles. Experimental and numerical velocities and skew angles were compared with theoretical predictions and good agreement was observed.

Keywords: Lamb waves, CFRP, BVID, Finite Element Modelling, Anisotropy, Wave skew, Beam spreading

1. INTRODUCTION

Carbon fiber reinforced laminates are increasingly used for lightweight aerospace applications. Unlike their metallic counterparts, carbon fiber laminates are highly anisotropic with high stiffness along the fiber directions, but they exhibit poor interlaminar strength [1]. This means that composite laminates are vulnerable to subsurface damage from low velocity impacts, which can significantly reduce structural integrity [2]. Accurate damage detection is required to maintain the safety of aircraft components. Ultrasonic guided waves are a promising structural health monitoring (SHM) technique for composites as they propagate along structures, enabling rapid, long-range inspection of large areas [3]. However, guided wave propagation is influenced by material anisotropy resulting in a number of effects including energy focusing [4], directional dependency of wave velocities [5], wave skewing, and beam spreading [6, 7]. If unaccounted for, these anisotropic effects could lead to inaccurate damage localization; therefore, understanding guided wave propagation behavior in anisotropic structures is required for accurate and reliable SHM of composites.

Guided wave velocities in anisotropic plates are both direction and frequency dependent. This results in three-dimensional dispersion curves and increases the complexity for damage detection. In unidirectional CFRP the S_0 mode exhibits the most significant directional variation [8]. Whilst the A_0 mode has lower directional variation, this is still significant enough to impact damage detection [9]. The directional dependency of group velocity has been well established [5, 10–14] , however equivalent studies for the phase velocity are limited [15].

In anisotropic plates the phase and group directions are not equal, and therefore wave energy tends to be focused away from the wave launching directions towards the fiber directions [16]. The extent of the steering of the wave packet can be defined by the wave skew angle, which is the angular difference between the group and phase directions. The group direction can be obtained by taking the normal to the phase slowness curve [17]. Skew angles of up to 40° have been predicted in composite laminates [15]. Chapuis et al. analytically predicted the energy focusing of Lamb modes in anisotropic plates [4]. Potel et al. determined theoretical wave skew angles using plane wave decomposition and found good agreement with experimental results [18]. Lowe et al. experimentally measured wave skew in a single wave launching

Health Monitoring of Structural and Biological Systems XVII, edited by
Paul Fromme, Zhongqing Su, Proc. of SPIE Vol. 12488, 1248804
 · 0277-786X · doi: 10.1117/12.2657435

direction in a unidirectional plate and found good agreement with theoretical predictions [8]. Salas and Cesnik demonstrated wave skewing experimentally through wavefield images of unidirectional, cross-ply and quasi-isotropic laminates, however skew angles were not quantified [19].

In this contribution the directional dependency of phase velocity and wave skew angles are investigated for the A_0 guided wave mode in an undamaged unidirectional CFRP panel through both experiment and Finite Element (FE) simulation. Experimental and FE results are compared to theoretical predictions obtained from dispersion curves throughout. The directional dependency of phase velocity is demonstrated, and the influence of wave skewing on phase velocity is described for a point source excitation. A line transducer was developed to measure wave skew angles in different wave launching directions and good agreement with both FE and theoretical predictions was obtained.

2. METHODOLOGY

Guided wave propagation in a unidirectional CFRP plate was investigated through both FE modelling and experimental measurements. Full 3D FE models of an undamaged unidirectional plate section with dimensions 400mm x 600mm x 3.6mm were performed in ABAQUS/Explicit. The plate was modelled as an anisotropic, homogenized structure with material properties as given in Table 1. Eight node solid brick elements (C3D8R) were selected for the model to generate a regular, uniform mesh. An element size of 0.5mm x 0.5mm x 0.45mm (eight elements through the plate thickness) was selected and the time increment and simulation time were set to 5ns and 150μs respectively, fulfilling the usual stability criteria. Stiffness proportional Rayleigh damping was incorporated into the model to simulate guided wave attenuation. The damping value was set to $\beta = 70$ns to match experimentally observed guided wave attenuation. Point source excitation of the A_0 mode was modelled by applying an out-of-plane force to a single node. The excitation signal was a 75kHz, 5 cycle sine wave modulated by a Hanning window. History outputs were defined along a line of points 100mm from the point excitation, in order to obtain simulated phase velocity values. Material properties were rotated in 5° increments from 0°-90° to achieve different wave propagation directions. In order to measure wave skew angles from the FE model, a line excitation was also modelled by applying simultaneous out-of-plane forces along a 40mm line of nodes. History outputs were defined along 5 lines of measurement points, perpendicular to the wave propagation direction, in order to capture the energy distribution of the wave pulse, as shown in Fig. 1a. Again, separate simulations were performed for each wave launching direction. Theoretical phase velocity dispersion curves were obtained from Disperse [20] for each wave launching direction using the material properties listed in Table 1. Phase velocity values were extracted at 75kHz for each direction. Wave skew angles were then calculated from the resulting slowness curve (inverse of phase velocity).

Experimental measurements were performed on a 3.6mm thick 24-ply undamaged unidirectional CFRP panel with material properties as given in Table 1. For approximate point source excitation of the A_0 mode, a piezoceramic transducer (lead zirconate titanate (PZT), Ferroperm Pz27, diameter 5mm, thickness 2mm) with a brass backing mass (diameter 5mm, thickness 6mm) was bonded to the plate surface. A programmable function generator was used to excite a 75kHz, 5 cycle sine wave modulated by a Hanning window. A laser vibrometer attached to a scanning rig was used to measure the velocity of the out-of-plane displacement at the plate surface. Retro-reflective tape was applied to the surface of the plate to improve laser beam reflection and subsequently the signal to noise ratio. Time signals were filtered using a band pass filter with cut-off frequencies of 50kHz and 100kHz, respectively. To measure the phase velocity of the A_0 mode in different wave launching directions, radial lines, 100mm length in 1mm steps, were scanned every 15° at a distance of 100mm from the transducer, as shown schematically in Fig. 1b.

Table 1: Orthotropic stiffness coefficients for the unidirectional CFRP laminate measured at 2MHz, obtained from [16]. Values in GPa unless otherwise stated.

C_{11}	C_{12}	C_{13}	C_{22}	C_{23}	C_{33}	C_{44}	C_{55}	C_{66}	ρ [kg/m^3]
12.56	6.84	6.47	13.15	5.6	109.9	4.7	4.0	2.27	1550

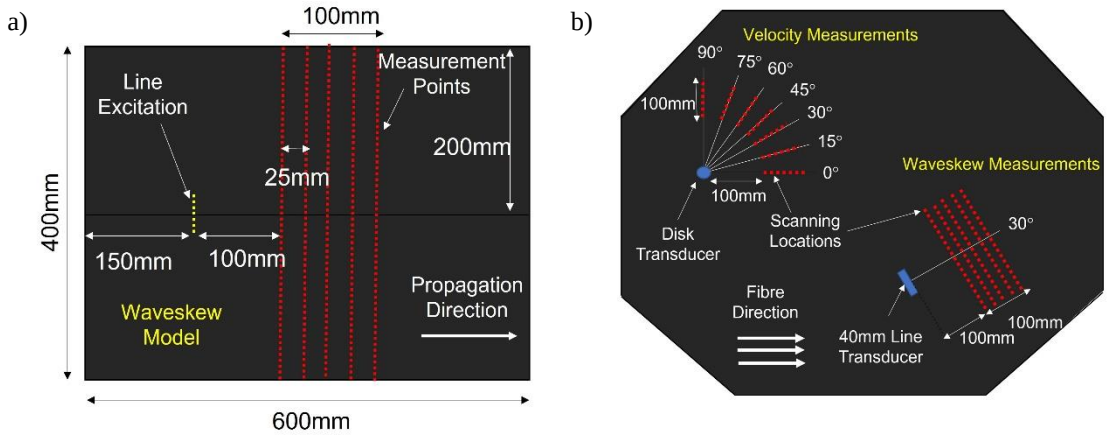

Figure 1: (a) Schematic of excitation and measurement locations of FE model for wave skew simulations; (b) schematic of transducer and measurement locations on the CFRP specimen.

To measure the wave skew angles in different wave launching directions a line transducer was developed. The transducer consists of a piezoelectric plate strip (PIC-255, dimensions 40mm x 5mm x 2mm) and a steel backing mass (dimensions 40mm x 5mm x 5mm), shown in Fig. 2a. Conductive tape was used to attach wires to the electrodes. To measure wave skew in different directions the transducer needs to be removable. Set honey was used as couplant and the transducer was clamped to the rear of the plate with a screw (Fig. 2b) to achieve repeatable clamping pressure. To test the repeatability of the clamping the line transducer was oriented along the 0° wave launching direction. A 200mm line of measurement points was scanned in 2mm steps 100mm from the transducer, perpendicular to the wave launching direction (parallel to the transducer). The transducer was removed, repositioned and the measurement repeated. The maximum Hilbert amplitude along the line of points was calculated for each measurement run and is shown in Fig. 2c. Each measurement shows a region of increased amplitude from approximately -40mm to +40mm ,with a main peak between approximately -40mm to +5mm. A sharp drop in amplitude can be observed at approximately +5mm, where an additional peak occurs. After considering the wavefield directly on top of the transducer, it was found that this peak is likely due to waves being excited from the end of the transducer. The overall shape of the excitation is reasonably repeatable, although there is some variation in amplitude, particularly for run 2. This is likely due to slight variations in the thickness of honey couplant and variations in the clamping position and pressure, which could not be fully eliminated. To measure wave skew angles, 5 parallel lines of measurement points were scanned at 100mm, 125mm, 150mm, 175mm, and 200mm from the line transducer as shown schematically in Fig. 1a. The lines were 300mm in length and scanned in 2mm steps. Measurements were repeated every 15° between 0° and 90°.

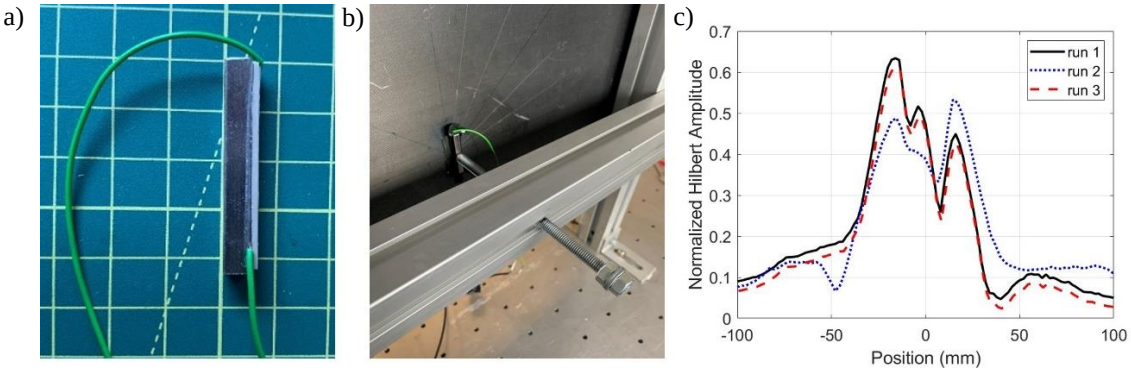

Figure 2: (a) Photograph of line transducer; (b) photograph of clamped line transducer; (c) repeatability of line excitation, Hilbert amplitude along line of measurement points 100mm from the transducer, 75kHz A_0 mode excitation frequency.

3. VALIDATION OF FE MODEL

To validate the FE models, experimentally measured phase velocities were compared with those calculated form the point source FE and theoretical values. The phase velocity was calculated for each measurement line by taking the FFT of each signal plotting the phase angle at the center frequency f (75kHz) against distance from the source, taking care to remove any 2π phase jumps. A linear fit was performed, and the gradient of the line extracted. Multiplying the inverse of this gradient by a factor of $2\pi f$ yields the phase velocity. This procedure was repeated for each wave propagation direction.

Figure 3 shows the directional dependency of phase velocity for the point source experiments, point source FE, and theory. Good agreement (within 1%) is observed between the point source FE and the experimental measurements indicating that the FE accurately captures the wave propagation behavior occurring in the physical specimen. Good agreement of phase velocity with theoretical values can be observed in the principal directions (0° and 90°), however in the non-principal directions a significant offset from the theoretical values can be observed (up to 12%). This offset is the result of wave skew effects. A larger offset is observed in wave launching directions with a larger skew angle, with the maximum offset occurring in the 45° direction. A correction can be applied to account for wave skew effects. The wave pulse measured in a given direction will have actually originated at a different phase direction and been steered due to anisotropy. To calculate the corrected velocity, the velocity along the corresponding group direction should be projected into the wave launching (phase) direction by multiplying by a factor of $\cos(\theta_{skew})$. For example, waves launched in the 45° direction have a skew angle of 25°, so taking the velocity measured in the 20° direction (group direction) and multiplying by $\cos(20°)$ will yield the correct velocity value.

The skew angle correction was applied to the experimental and FE point source phase velocities. The uncorrected velocities shown in Fig. 3 were obtained in 5° increments, so velocity values were linearly interpolated to obtain uncorrected values in 1° increments. The dashed lines in Fig. 3 show the corrected experimental (red) and FE (blue) phase velocity values. Very good agreement with the theoretical values can be seen, indicating that the skew angle correction can adequately compensate for beam skewing due to anisotropy.

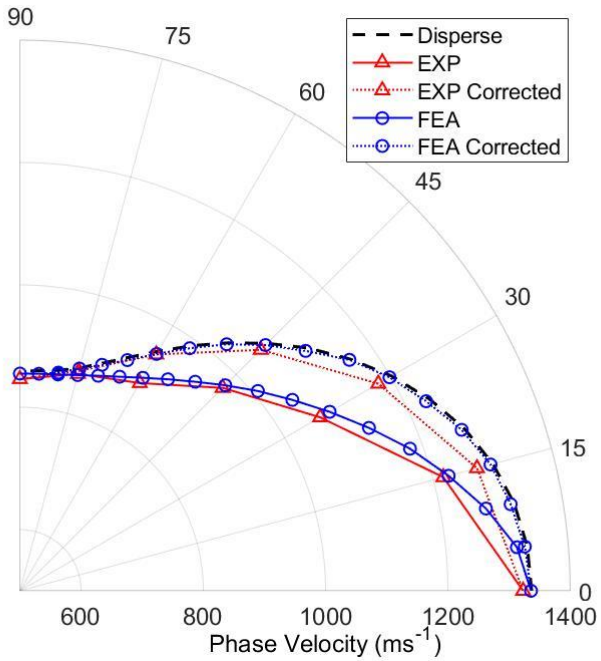

Figure 3: Directional dependency of A_0 mode phase velocity at 75kHz. Experimental, simulated, and theoretical values are shown in addition to corrected FE and experimental values.

4. WAVE SKEW ANGLE CALCULATION

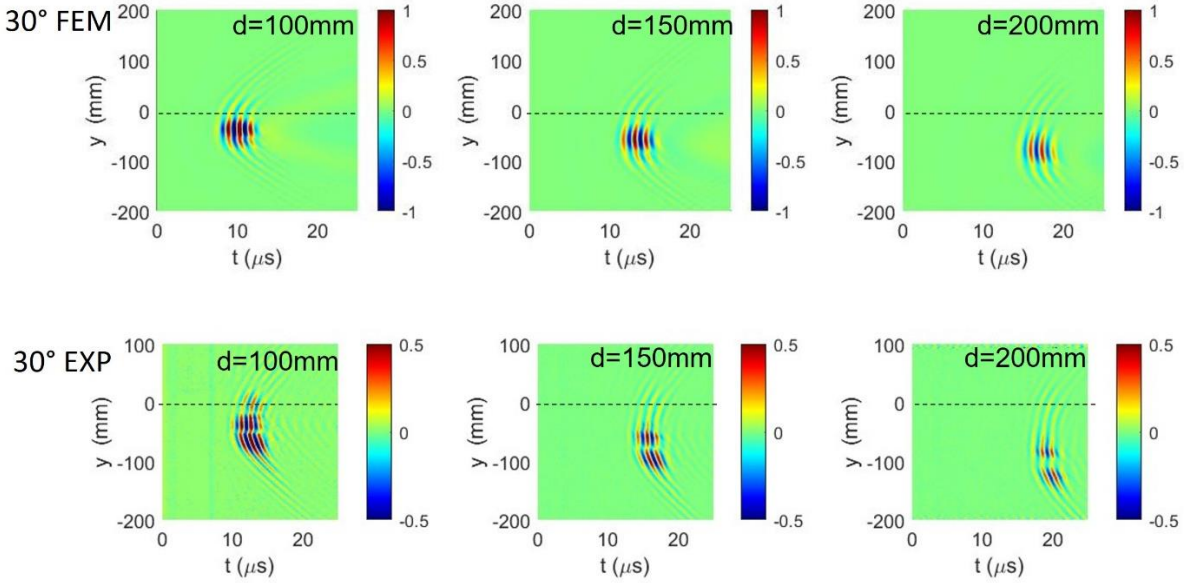

Figure 4: Normalised displacement time traces along single line of measurement points (parallel to line source) for the A_0 mode obtained from FE and experimental measurements. 30° wave launching angle, 3 lines of measurement points located 100mm, 150mm, and 200mm from line source. Wave launching direction represented by black dashed line at y=0mm.

Figure 4 visualizes time traces along lines of measurement points, equivalent to a B-scan, for both the experimental measurements and FE model in the 30° direction. The FE results (Fig. 4, top row) show that the wave pulse deviates from the wave launching direction (black dotted line) towards the fiber directions. In the experimental wavefields (Fig. 4, bottom row), the wave pulse consists of two regions of high amplitude, which is not observed in the FE model. Significant wave steering from the initial direction can be observed, consistent with the FE images. The line excitation in the experiments is imperfect with a region of low amplitude in the middle of the exaction. This could be caused by destructive interference at the center of the transducer, whose length is approximately twice the wavelength at 75kHz. In both the FE model and the experimental B-scans the wavefronts remain oriented along the phase direction (parallel to the line source orientation).

To quantify the wave skew angle, the aim is to track the position of the wave pulse y over distance d, which should vary linearly. The position of the wave pulse is then plotted against distance from the source and a linear fit performed. The gradient of the fit can then be extracted, and the skew angle calculated as:

$$\theta_{skew} = \tan^{-1}\left(\frac{\Delta y}{\Delta d}\right) \quad (1)$$

The position of the wave pulse can be determined by fitting a curve to the Hilbert amplitude distribution (similar to those in Fig. 2c) and determining the center of the pulse.

A variety of Gaussian and Lorentzian functions were fitted to the amplitude curves for each wave launching direction. For smooth amplitude curves a Gaussian function already provided a good fit, however in directions with multiple amplitude peaks a more complex fitting function was required to match the features. Figure 5 shows the fitted FE and experimental curves for the 30° wave launching direction for a Gaussian (Fig. 5a/b), Lorentzian (Fig. 5c/d), and a three term Gaussian curve (Fig. 5e/f). The sum of two Gaussian and two Lorentzian functions were also investigated, respectively; however, it was not possible to adequately fit these functions to either the experimental or FE data. The 30° wave launching direction is considered as this was the worst case in terms of pulse uniformity for both the measurement and FE simulation. The starting points for the MATLAB fitting algorithm were optimized for each propagation angle. As seen in Fig. 5a, fitting a Gaussian function to the FE data provides a reasonable fit ($R^2 > 0.94$), but does not capture the full peak amplitude or adequately account for the side peaks either side of the main peak. A Gaussian can be fitted to the dual peak in the experimental data (Fig. 5b) but the fit curve represents an average between the two peaks. Whilst the fitting was poor

($R^2 > 0.3$), taking the maximum of the Gaussian provided a surprisingly accurate wave skew angle. The Lorentzian fit in Fig. 5c visually provides a better match to the FE data than the Gaussian fit ($R^2 > 0.97$), however this function provides an extremely poor fit for the experimental data in Fig. 5d. The three term Gaussian fit shown in Fig. 5e provides a very good match for the FE curves, accounting for the side peaks as well as fitting the main peak very well ($R^2 > 0.99$). Additionally, the three term Gaussian fits the dual peak in the experimental measurements well and provided the best fit ($R^2 > 0.98$) for all cases.

Skew angles were calculated from both the single Gaussian, and three term Gaussian functions. In order to estimate the position of the wave pulse the weighted sum of three standard Gaussian functions was fitted to each experimental and FE amplitude curve:

$$f(x) = a_1 \exp\left[-\left(\frac{x-b_1}{c_1}\right)^2\right] + a_2 \exp\left[-\left(\frac{x-b_2}{c_2}\right)^2\right] + a_3 \exp\left[-\left(\frac{x-b_3}{c_3}\right)^2\right] \quad (2)$$

where the coefficients a_n represent the amplitude of each Gaussian peak, the coefficients b_n represent the centroid of each peak, and coefficients c_n are related to the width of each peak. The first term of this equation expresses the single Gaussian function. To estimate the true center of the wave pulse, a weighted average of the peak centroids was performed (i.e., b_n weighted with respect to a_n).

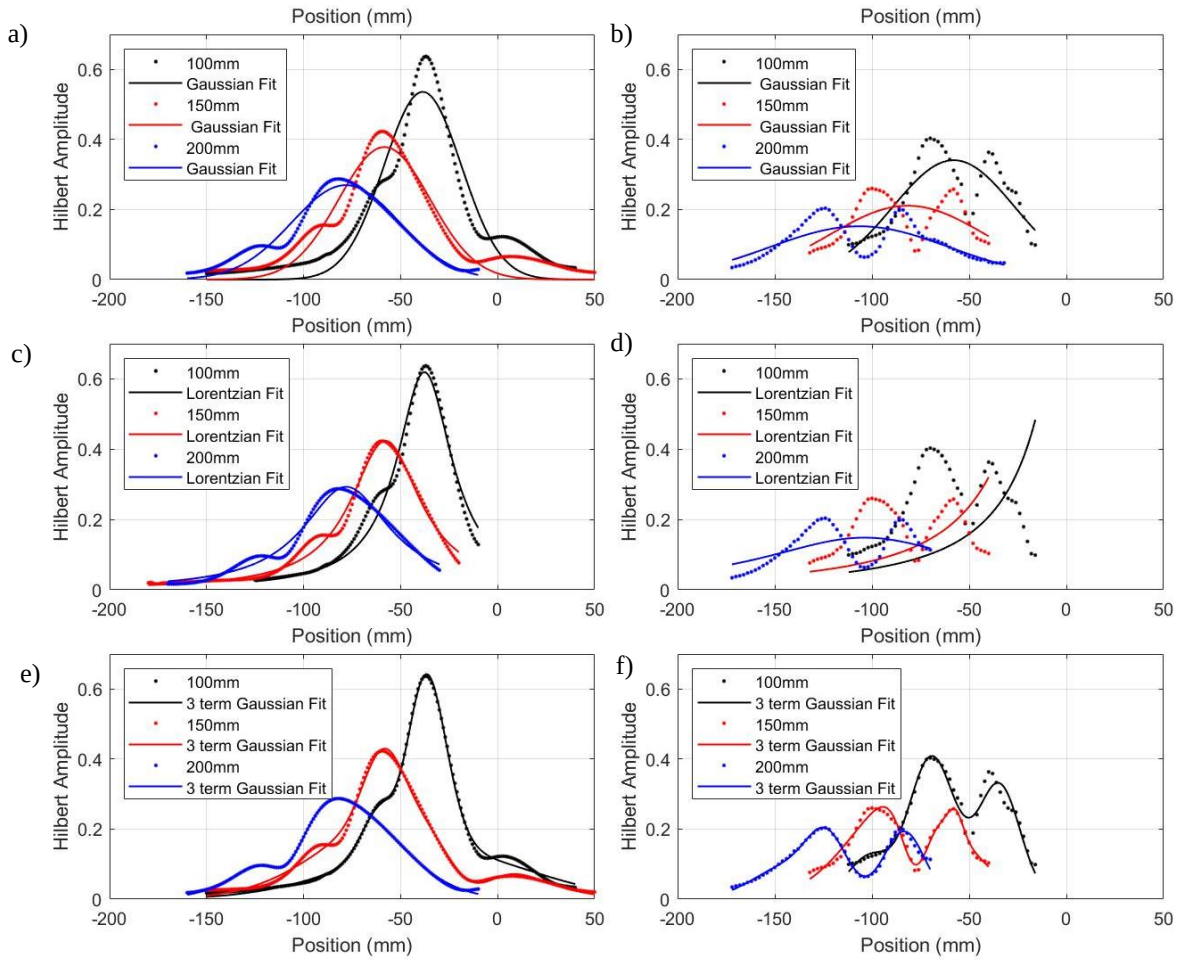

Figure 5: Measured and simulated amplitude curves with various curve fitting functions, 30° wave launching direction
a) single Gaussian fit to FE data; b) single Gaussian fit to experimental data; c) single Lorentzian fit to FE data;
d) single Lorentzian fit to experimental data; e) three term Gaussian fit to FE data; f) three term Gaussian fit to experimental data.

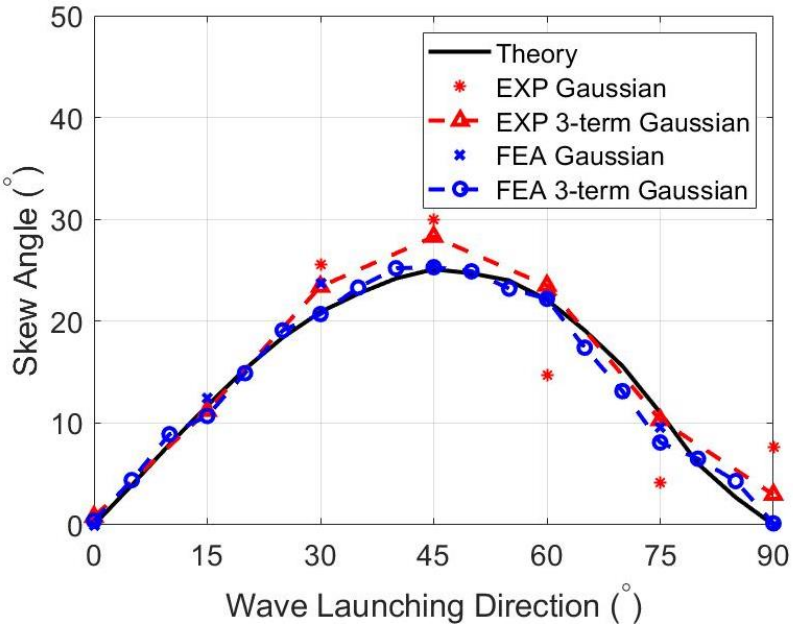

Figure 6: Angular dependency of wave skew angle of A_0 mode at 75kHz. Experimental and FE values are shown for both the Gaussian and three term Gaussian analysis, and compared with theoretical values obtained from phase slowness curves.

The skew angles obtained from the experimental measurements and FE simulations, calculated from the two different fits are shown in Fig. 6 in addition to the theoretical values obtained from the phase slowness curves. The theoretical values (black solid) show zero skew angle in the principal directions (0°/90°) as expected from the material anisotropy. As the wave launching direction deviates from the principal directions, the wave skew angle increases until a maximum skew angle of 25° in the 45° wave launching direction. The skew angles are fairly symmetric about the 45° direction, with the slight difference being due to energy focusing effects being more dominant for the 0°-45° directions, whereas beam spreading effects significantly affect wave propagation in the 45°-90° directions. The different analyses of the FE simulation data give similar skew angles, except for in the 30° direction, where the three term Gaussian analysis is in closer agreement with theory. Overall good agreement with the theoretical skew angles is achieved. The skew angles from the single Gaussian analysis provide surprisingly good agreement with the theoretical values at low wave launching angles, however above 30° significant discrepancy with the theory is observed. On the other hand, the experimental results from the 3-term Gaussian analysis show reasonable agreement with the theoretical predictions. However, in directions with high wave skew, the measured angles are overestimated. As the experimentally measured point source velocities showed good agreement with theory for the skew angle correction, it is unlikely that the error in skew angle is due to incorrect material properties. The experimental error in the wave skew angles could be caused by the quality of the line source excitation. It should be noted that the anisotropic wave propagation effects in a unidirectional laminate will be larger than that of a cross-ply or quasi-isotropic CFRP layup. The beam steering in these laminates will be smaller but could still be significant enough to reduce the accuracy of guided wave based SHM.

5. CONCLUSIONS

Anisotropic wave propagation effects of the A_0 guided wave mode were investigated for a unidirectional CFRP laminate through both experiments and FE simulation. Both directional dependency of phase velocity and wave skewing were considered, and good agreement was found between FE simulation and experimental results. Phase velocities measured from a point source excitation need to be corrected for wave skewing effects that occur in anisotropic materials, otherwise a significant offset occurs from theoretical values for high skew directions. A line transducer was developed and demonstrated to have consistent repeatable coupling and was used to experimentally measure wave skew angles. Good agreement with theoretical values obtained from phase slowness curves was achieved. Understanding anisotropic wave propagation effects is essential for the SHM of composite structures, as they could lead to errors in damage localization if not considered in the development and analysis of SHM methodology and algorithms.

REFERENCES

[1] K. Hayat, S.K. Ha, Low-velocity impact-induced delamination detection by use of the S0 guided wave mode in cross-ply composite plates: A numerical study, Journal of Mechanical Science and Technology. 28 (2014) 445–455.

[2] T.W. Shyr, Y.H. Pan, Impact resistance and damage characteristics of composite laminates, Compos Struct. 62 (2003) 193–203.

[3] K. Diamanti, J.M. Hodgkinson, C. Soutis, Detection of low-velocity impact damage in composite plates using lamb waves, Struct Health Monit. 3 (2004) 33–41.

[4] B. Chapuis, N. Terrien, D. Royer, Excitation and focusing of Lamb waves in a multilayered anisotropic plate, J Acoust Soc Am. 127 (2010) 198–203.

[5] O. Putkis, R.P. Dalton, A.J. Croxford, The anisotropic propagation of ultrasonic guided waves in composite materials and implications for practical applications, Ultrasonics. 65 (2016) 390–399.

[6] P. Fromme, M. Pizzolato, J. Robyr, B. Masserey, Lamb wave propagation in monocrystalline silicon wafers, J Acoust Soc Am. 143 (2018) 287–295.

[7] F. Hervin, P. Fromme, Guided wave propagation and skew effects in anisotropic cfrp laminates, Submitted Manuscript. (2022).

[8] M.J.S. Lowe, G. Neau, M. Deschamps, Properties of Guided Waves in Composite Plates, and Implications for NDE, AIP Conf Proc. 700 (2004) 214–221.

[9] F. Hervin, P. Fromme, Anisotropy influence on guided wave scattering for composite structure monitoring, Structural Health Monitoring (2022).

[10] A. de Luca, D. Perfetto, A. Polverino, A. Aversano, F. Caputo, Finite Element Modeling Approaches, Experimentally Assessed, for the Simulation of Guided Wave Propagation in Composites, Sustainability 14 (2022).

[11] J. Zhao, J. Qiu, H. Ji, Reconstruction of the nine stiffness coefficients of composites using a laser generation based imaging method, Compos Sci Technol. 126 (2016) 27–34.

[12] S.H. Rhee, J.K. Lee, J.J. Lee, The group velocity variation of Lamb wave in fiber reinforced composite plate, Ultrasonics. 47 (2007) 55–63.

[13] L. Wang, F.G. Yuan, Group velocity and characteristic wave curves of Lamb waves in composites: Modeling and experiments, Compos Sci Technol. 67 (2007) 1370–1384.

[14] G. Neau, M. Deschamps, M.J.S. Lowe, Group velocity of Lamb waves in anisotropic plates: Comparison between theory and experiments, AIP Conf Proc. 557 (2001) 81–88.

[15] H. Gao, Ultrasonic guided wave mechanics for composite material structural health monitoring, PhD Thesis, The Pennsylvania State University, 2007.

[16] G. Neau, M.J.S. Lowe, M. Deschamps, Propagation of Lamb waves in anisotropic and absorbing plates: Theoretical derivation and experiments, AIP Conf Proc. 615 (2002) 1062–1069.

[17] J.L. Rose, Ultrasonic guided waves in solid media, Cambridge University Press, 2014.

[18] C. Potel, S. Baly, J. de Belleval, M. Lowe, P. Gatignol, Deviation of a Monochromatic Lamb Wave Beam in Anisotropic Multilayered Media: Asymptotic Analysis, Numerical and Experimental Results, IEEE Trans Ultrason Ferroelectr Freq Control. 52 (2005) 987–1001.

[19] K.I. Salas, C.E.S. Cesnik, Guided wave structural health monitoring using CLoVER transducers in composite materials, Smart Mater Struct. 19 (2010) 015014.

[20] B. Pavlakovic, M. Lowe, D. Alleyne, P. Cawley, Disperse: A General Purpose Program for Creating Dispersion Curves, Review of Progress in Quantitative Nondestructive Evaluation. 16 (1997) 185–187.